1. EPR characterization

The electron resonance (EPR) measurements were made at room temperature using a Bruker EMX-10/12-type spectrometer in the X-band.

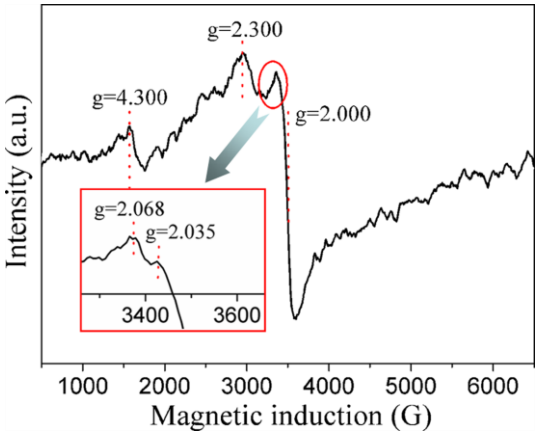

Fig. S1 EPR characterization of iron oxide/H_2O_2 system

Six EPR peaks can be found in S1: g = 4.3, g = 2.3, g = 2.035, g = 2.068 and g = 2. In these peaks, the peaks of g = 4.3, g = 2.3, g =2 are the characteristic peaks of iron oxide, which has been reported in many other papers [1,2]. The peaks of g = 2.068 and g = 2.035 can be assigned to the peak of hydroxyl radical. The location of the peak is very near to the superoxide radical, which has been reported in other papers [3,4]. The low intensity of this peak is due to the instability of hydroxyl radical.

2. Confirmation of free radical reaction

In order to further confirm that the NO_X removal is resulted by ·OH oxidation reaction. A series of experiments were conducted. In the NO_X removal process, the free radical terminator, isopropanol, was injected into the fixed bed. Results are shown in S2.

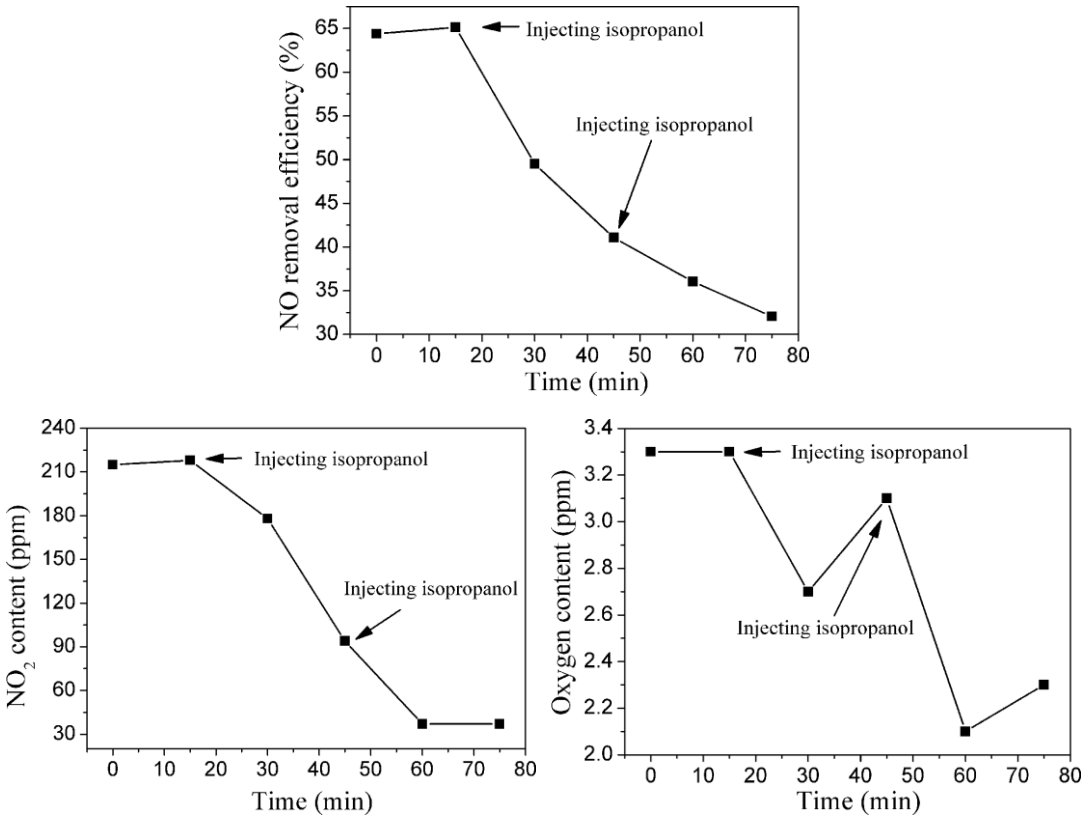

S2 Variation of NO removal efficiency, NO_2 content and oxygen content after injecting isopropanol

It can be seen from S2 that both the NO_X removal efficiency and NO_2 content decline after injecting isopropanol into fixed bed, it indicates that this reaction is free radical reaction, and the isopropanol reacts with the hydroxyl free radicals to form stable free radicals. And these stable free radicals can not remove NO_X, can not oxidize NO_2 and can not generate O_2.

3. Characterization of ion chromatography

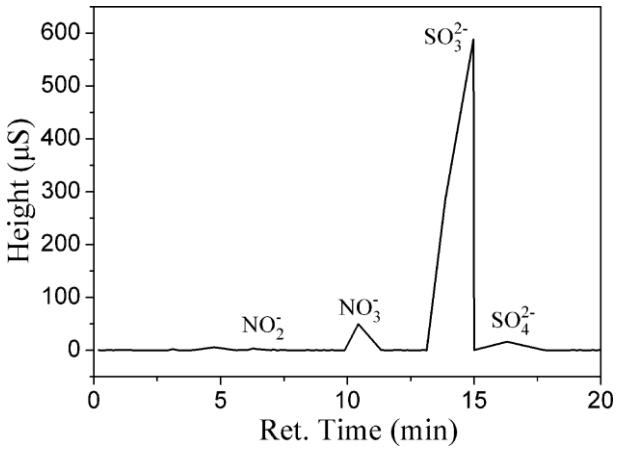

S3 Ion chromatography of absorbent

The peak of NO_2^- and SO_4^{2-} is very weak comparing with the peak of NO_3^- and SO_4^{2-}, and the concentration of NO_2^- and SO_4^{2-} can be neglected in this paper.

4. TPD of different Fe based catalysts

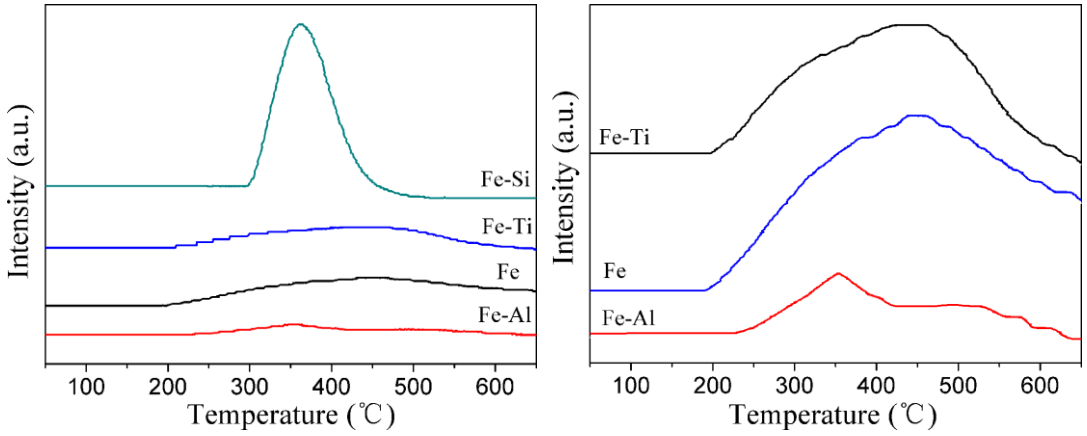

S4 NH_3-TPD characterization of Fe based catalysts

From S4 (a) and (b), we can find that the acidic sites of catalysts decreased as follows: Fe-Si > Fe > Fe-Ti > Fe-Al. But the NO_X removal efficiency decreased as follows: Fe > Fe-Al > Fe-Ti > Fe-Al. Thus, the theory of acidic and alkaline sites can not explain the observed phenomenon definitely.

5. The variation of oxygen content with temperature of simulated flue gas with different catalysts.

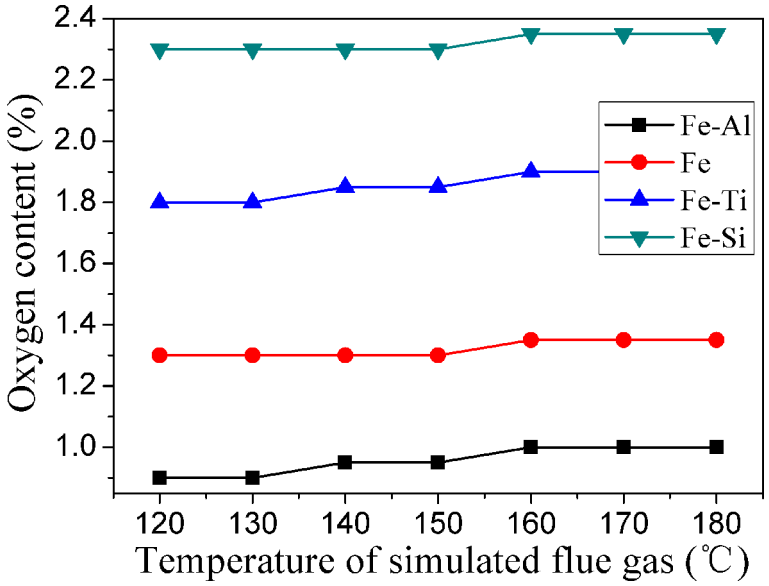

S5 Variations of oxygen content with temperature of simulated flue gas at different catalysts

From S5, we can find that the oxygen content decreases as the following order: Fe-Si > Fe-Ti > Fe > Fe-Al.

6. Characterization of XRD

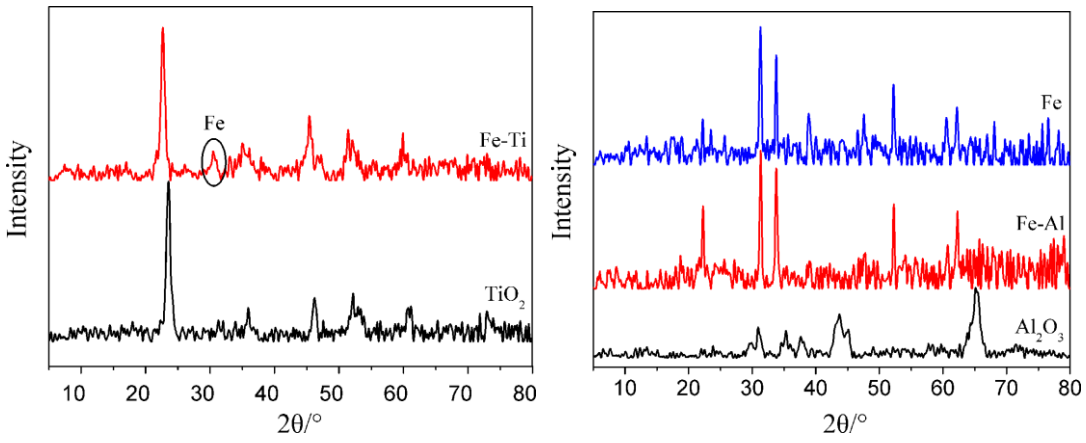

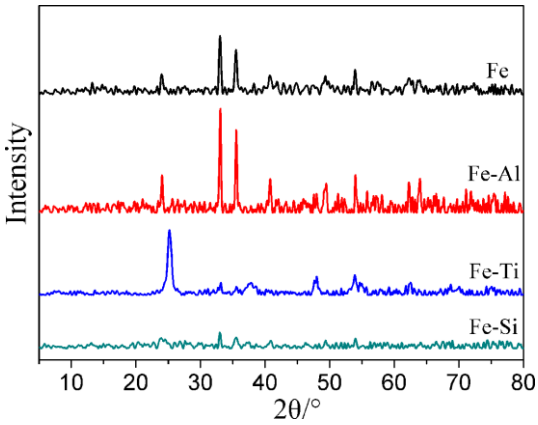

S6 XRD characterizations of TiO_2, Al_2O_3, Fe, Fe-Al, Fe-Ti, Fe-Si

From S6, it can be found that the main peaks of hematite in Fe-Ti and Fe-Si are very weak. But in Fe and Fe-Al, characteristic peaks of hematite can be obviously observed.

7. Ion chromatographs

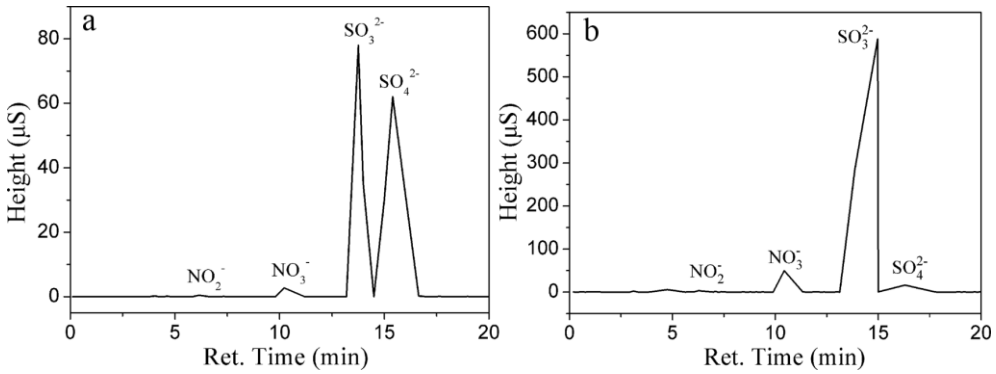

S7 Ion chromatographs of solution in the inlet of absorber (a) and the absorbent (b)

In S7, the sulfite ratio in sulfite and sulfate remains high in solution in the inlet of absorber and the absorbent. This means the low concentration of H_2O_2 in solution, and most of H_2O_2 is decomposed over the Fe based catalysts.

8. Porous structure parameters of different catalysts

Table S1 Porous structure parameters of different catalysts

Sample	BET surface area (m^2/g)	Total pore volume (cm^3/g)
Fe	45.31	0.122
Fe-Al	44.71	0.172
Fe-Ti	47.30	0.138
Fe-Si	45.03	0.127

9. Experimental

Synthesis

The catalyst support (Titania, Silica and Magnesia) was prepared by precipitation method[5-7]. The iron oxide loading catalyst was impregnated by incipient wetness with aqueous solution of 25% (mol/mol) ferric nitrite. The impregnated catalyst was first dried at 120℃ for 4 h followed by calcinations at 550℃ in air for 5 h. The percent of metals Fe is based on support[8]. The pure iron oxide catalyst was prepared by $Fe(NO_3)_3 \cdot 9H_2O$ (Sinopharm Chemical Reagent Co., Ltd, AR). Ferric nitrate was mixed in the 100 ml deionized water under agitating with magnetic stirrer at 80℃ until the water is dried. The obtained substance was firstly dried at 120℃ for 4h followed by calculations at 550℃ in air for 5h. The iron oxide loading on the titania, alumina, silica, magnesia and pure iron oxide catalyst is denoted as Fe-Ti, Fe-Al, Fe-Si, Fe-Mg and Fe, respectively.

10. Charaterization

Decomposition of H_2O_2

0.2 g catalyst was mixed into 10 ml 30 wt% H_2O_2 solution under agitating with magnetic stirrer for 30 min to reach equilibrium. Then the solution was centrifuged and 4 ml of the supernatant was mixed into 50 ml deionized water. The potassium permanganate ($KMnO_4$) solution with the concentration of 0.01 $mol \cdot L^{-1}$ was used to titrate the above supernatant. The consummated $KMnO_4$ was used to represent the decomposed H_2O_2 in the solution.

Concentration of iron ions

The concentration of iron ions is detected with titration method. Firstly, we obtained the solution with the above method. And then the EDTA solution with the concentration of 0.001 $mol \cdot L^{-1}$ was used to titrate the supernatant. The consummated EDTA was used to calculate the concentration of iron ions in the solution.

Characterization of catalyst

The power X-ray diffraction (XRD) measurement was carried out with Beijing Purkinjie general instrument XD-3 X-ray diffraction (CuKα, voltage 35 kV, electrical current 20 mA, 2θ from 5° to 80°). Microstructures of the catalyst were observed by scanning electron micrograph (SEM) in JEOLJSM-6380LV (Japan) system at a voltage of 20 kV. Specific surface area was measured using nitrogen adsorption at -196℃ and determined by BET method using a V-Sorbet 2800S automated gas sorption system. XPS experiments were carried out on a RBD upgraded PHI-5000C ESCA system (Perkin Elmer) with Mg Kα radiation ($h\nu$ = 1253.6 eV), calibrated by the C 1s peak at 284.6 eV with an accuracy of 0.2 eV. The pzc values were measured

with a mass titration method [9,10].

Ammonia temperature-programmed desorption (NH_3-TPD) experiments were performed in a flow of He (30 $cm^3 \cdot min^{-1}$) over 200 mg of catalyst using a heating rate of 8 ℃$\cdot min^{-1}$. Prior to the TPD experiments, the catalysts were preheated under a flow of He at 400 ℃ for 1 h, followed by cooling down to room temperature in the same flow. The NH_3 adsorption was conducted with the flow rate of 20 $ml \cdot min^{-1}$ at room temperature.

The surface acidity of the catalysts was investigated by means of a Fourier transform infrared spectroscopic (FTIR) study of ammonia (NH_3) absorption. NH_3 FT-IR spectra were recorded in a IS10 FTIR spectrometer. The samples were absorbed by NH_3 for 5 h. Then, the spectra (200 scans, resolution: $1cm^{-1}$, range of acquisition: 650-4000 cm^{-1}) were recorded after evacuation (10^{-5} Torr or 0.0013 Pa) for 30 min.

11. Economic calculation

The price of 30% H_2O_2 is about 246 dollars/T. The 70% NO_X removal efficiency is used to be calculated. The cost of NO_X removal is only about 0.6782 dollars/g NO_X. It is supposed that the price of energy consummation is about 0.08 dollars/Wh. The cost of energy consummation is only about 8.477 Wh/g (NO_X). Tseng et al.[11] have investigated the combined removal of NO_X and SO_2 from simulated flue gas in a bench-scale pulsed-corona enhanced wet electrostatic precipitator with the addition of ammonia (NH_3) and ozone (O_3). The maximum removal rates for NO_X and SO_2 were

77% and 99%, respectively, with injection of 312ppm O_3 and 2900ppm NH_3. The energy consumption rates were as high as 38.6 Wh/g (NO_X). The energy consumption in the study by Tseng et al. is 4.56 times higher than that obtained in the simultaneous flue gas desulfurization and denitrification with H_2O_2 in the present study (8.477 Wh/g). Saavedra et al.[12] investigated NO_X treatment using DBD without additional catalysts or oxidants, and the NO_X removal rate reached 98%. It should be noted that only denitrification was performed in this study, and no desulfurization occurred. The NO_X energy consumption rate (875 Wh/g) was 103 times higher than the simultaneous flue gas desulfurization and denitrification method with this study in the paper.

12. The undetectability of Fe(IV)

According to the Pham's mechanism as follows:

The radical mechanism

$$\equiv Fe(III)+H_2O_2 \rightarrow \equiv Fe(II)+HO_2^{\bullet}(O_2^{\bullet-})+H^+(2H^+)$$

$$\equiv Fe(II)+H_2O_2 \rightarrow \equiv Fe(III)+{\bullet}OH+OH^-$$

$$HO_2^{\bullet} \rightleftharpoons H^+ + O_2^{\bullet-}$$

$$\equiv Fe(III)+HO_2^{\bullet}(O_2^{\bullet-}) \rightarrow \equiv Fe(II)+O_2(+H^+)$$

The non-radical mechanism

$$\equiv Fe(III)+H_2O_2 \rightarrow \equiv Fe(II)+HO_2{\bullet}+H^+$$

$$\equiv Fe(II)+H_2O_2 \rightarrow Fe(IV)+2OH^-$$

$$\equiv Fe(IV)+H_2O_2 \rightarrow \equiv Fe(II)+O_2+2H^+$$

$$\equiv Fe(IV)+\equiv Fe(II) \rightarrow 2\equiv Fe(III)$$

$$\equiv Fe(III)+HO_2^{\bullet}(O_2^{\bullet-}) \rightarrow \equiv Fe(II)+O_2(+H^+)$$

From the above mechanism, it can be found that the generation of oxygen is along with the generation of Fe(IV). Thus, maybe the generation of oxygen can be detected by the content of Fe(IV) using XPS characterization. However, previous papers[13] have reported the undetectability of Fe(IV), because the XPS characteristic peaks of Fe(IV) are coincident with those of Fe(II).

13. XPS results of fresh and reacted Fe-Ti and Fe-Al

Table S2 XPS results of fresh and reacted Fe-Ti and Fe-Al

Samples	Surface atomic concentration (%)			
	Fe		O	
	Fe(III)	Fe(III)OH	O	-OH
Fe-Ti	38.28	9.88	51.05	48.95
Fe-Al	31.88	20.69	68.93	31.07

[1] G. Ennas, A. Musinu, G. Piccaluga, D. Zedda, Characterization of iron oxide nanoparticles in an Fe_2O_3-SiO_2 composite prepared by a sol-gel method, Chem. Mater. 10 (1998) 495-502.

[2] M.S. Kumar, M. Schwidder, W. Grünert, A. Brückner, On the nature of different iron sites and their catalytic role in Fe-ZSM-5 $DeNO_X$ catalysis: new insights by a combined EPR and UV/VIS spectroscopic approach, J. catal. 227 (2004) 384-397.

[3] E. Carter, A.F. Carley, D.M. Murphy, Evidence for O_2^- radical stabilization at surface oxygen vacancies on polycrystalline TiO_2, J. Phys. Chem. C 111 (2007) 10630-10638.

[4] A. Adamski, B. Gil, Z. Sojka, Role of vanadium sites in NO and O_2 adsorption process over VO_X/CeO_2-ZrO_2 catalysts-EPR and IR studies. Catalysis Today 137 (2008) 292-299.

[5] J. Lv, L. Qiu, B. Qu, Controlled growth of three morphological structures of magnesium

hydroxide nanoparticles by wet precipitation method. Journal of Crustal Growth 267 (2004) 676-684.

[6] Riteer, H.S., 1960. Silica precipitation method. US Patent 2,921,839.

[7] R. Zhang, Q. Zhong, W. Zhao, L. Yu, H. Qu, Promotional effect of fluorine on the selective catalytic reduction of NO with NH_3 over CeO_2-TiO_2 catalysts at low temperature. Applied Surface Science (2013), DOI: 10.1016/j.apsusc.2013.10.143. (In press).

[8] J.A. Navío, G. Colón, M. Trillas, Heterogeneous photocatalytic reactions of nitrite oxidation and Cr(VI) reduction on iron-doped titania prepared by the wet impregnation method. Applied Catalysis B: Environmental 16 (1998), 187-196.

[9] J.S. Noh, J.A. Schwarz, Estimation of the point of zero charge of simple oxides by mass titration. Journal of Colloid and Interface Science 130 (1989) 157-164.

[10] J.S. Noh, J.A. Schwarz, Effect of HNO_3 treatment on the surface acidity of activated carbons. Carbon 28 (1990) 675-682.

[11] C.H. Tseng, T.C. Keener, Enhanced effect of in-situ generated ammonium salts aerosols on the removal of NO_X from simulated flue gas. Environmental Science and Technology 35 (2001) 3219-3224.

[12] H.M. Saavedra, M.P. Pacheco, J.O. Paceco-Sotelo, C.E.T. Reyes, J.A.D. Gomez, Modeling and experimental study on nitric oxide treatment using dielectric barrier discharge. IEEE Transactions on Plasma Science 35 (2007) 1533-1540.

[13] P. Deplano, E.T. Trogu, Sythesis and magnetochemical, spectroscopic, and structural studies of new Tris(N,N-dialkyldiselenocarbamato) iron (IV) tetrafluoroborate complexes. Journal of the Chemical Society, Dalton Transactions 1 (1983) 25-30.